Multi-Linear Probabilistic Energy Flow Analysis of Integrated Electrical and Natural-Gas Systems

Sheng Chen, *Student Member, IEEE*, Zhinong Wei, Guoqiang Sun, *Member, IEEE*, Kwok W. Cheung, *Fellow, IEEE*, and Yonghui Sun

***Abstract*—The deep interdependence between electrical and gas systems entails a potential threat to the security (or reliability) of both systems. It is imperative to investigate the impacts of massive uncertainties on the overall secure and economical operation of both systems. In this paper, a probabilistic energy flow framework of integrated electrical and gas systems is initially proposed considering correlated varying energy demands and wind power. Three aspects of couplings between electrical and gas systems are considered: gas-fired generators, electric-driven compressors, and energy hubs integrated with power to gas (P2G) units. Furthermore, a multilinear method is specially designed to produce a deterministic energy flow solution for each sample generated by Monte Carlo simulation (MCS). Finally, test results have verified that the proposed multilinear MCS method prevails over the nonlinear MCS. In addition, P2G effectively benefits the operation of both electrical and gas networks.**

***Index Terms*—Integrated electrical and gas systems, Monte Carlo simulation (MCS), multi-linear method, power to gas (P2G), probabilistic energy flow analysis.**

NOMENCLATURE

Variables

V_i	Voltage magnitude of node *i*
θ_i	Voltage angle of node *i*
$P_{\rm ij}$, $Q_{\rm ij}$	Active and reactive power flow through branch *i-j*
P_G, Q_G	Active and reactive power outputs of generators.
P_L, Q_L	Active and reactive power loads.
Δf	Frequency deviation.
π_m	Gas pressure of node *m*
F_w	Gas flow through pipeline *w*
$F_{\rm c}$	Gas flow through compressor *c*
$H_{\rm c}$	Horsepower of compressor *c*
τ_c	Gas consumed by compressor *c*
F_S	Gas injections of gas sources
F_D	Gas withdraws of gas demands
F_G	Gas consumption of gas-fired generators
P_e, P_g	Input electric power and gas of energy hub
L_e, L_h	Electricity and heat demands of energy hub
X	Vector of energy flow state variables
Y	Vector of energy flow injections
J	Jacobian matrix
$F_{D,\rm tot}$	Total equivalent gas demand

Parameters and Constants

$g_{\rm ij}$, $b_{\rm ij}$	Series conductance and susceptance of branch *ij*
$g_{{\rm sh},i}$, $b_{{\rm sh},i}$	Shunt values of bus *i*
K_G	Change rate in active power outputs with respect to Δf
$P_{G\_\rm set}$, $Q_{G\_\rm set}$	Specified active and reactive power outputs of generators
a_Q, b_Q	Coefficients of the generators' reactive power outputs
K_P, K_Q	Change rate in active and reactive power loads with respect to frequency deviation
$P_{L\_\rm set}$, $Q_{L\_\rm set}$	Specified active and reactive power demands
$V_{\rm LB}$	Nominal voltage magnitude of the load bus
k_w	Weymouth constant of gas pipeline *k*
α, β, γ	Gas consuming parameters of gas-fired compressors
T_S	Node-gas source incidence matrix
T_D	Node-gas demand incidence matrix
T_c	Node-gas turbine incidence matrix
A_w	Node-pipeline incidence matrix
A_c	Node-compressor incidence matrix
$\alpha_g, \beta_g, \gamma_g$	Energy conversion parameters of gas-fired generators
v_1	Percentage of electricity fed into P2G
v_2	Percentage of gas fed into CHP
$\eta_{\rm ee}$	Transformer efficiency
$\eta_{{\rm CHP},e}$, $\eta_{{\rm CHP},h}$	Gas-electric and gas-thermal efficiency of CHP
$\eta_{\rm eg}$	P2G efficiency
$\eta_{\rm gh}$	Gas furnace efficiency
C	Coupling matrix of energy hub
T_g	Gas node-energy hub incidence matrix
$T_{\rm gg}$	Gas node-generator incidence matrix
$r_{\rm ij}$, $x_{\rm ij}$	Resistance and reactance of branch *ij*
ρ_1	Electricity-gas demand correlation
ρ_2	Electricity-heat demand correlation
ρ_3	Heat-gas demand correlation

Manuscript received December 28, 2015; revised April 21, 2016 and June 25, 2016; accepted July 24, 2016. Date of publication August 4, 2016; date of current version April 17, 2017. This work was supported by the National Natural Science Foundation of China under Grant 51277052. Paper no. TPWRS-01853-2015. *(Corresponding author: Zhinong Wei.)*

S. Chen, Z. N. Wei, G. Q. Sun, and Y. H. Sun are with the College of Energy and Electrical Engineering, Hohai University, Nanjing 210098, China (e-mail: chenshenghhu@163.com; wzn_nj@263.net; hhusunguoqiang@163.com; sunyonghui168@gmail.com).

K. W. Cheung is with GE Grid Solutions, Redmond, WA 98052 USA (e-mail: kwok.cheung@ge.com).

Color versions of one or more of the figures in this paper are available online at http://ieeexplore.ieee.org.

Digital Object Identifier 10.1109/TPWRS.2016.2597162

I. Introduction

With an increasing penetration of natural-gas fired generators and the promising usage of power to gas (P2G) technology [1], [2], the interdependence between electrical and gas systems is strong and accelerating [3], [4]. Based on this background, it is imperative to model the electrical and gas networks as an integrated energy system [5], [6].

Renewable energy sources are projected to play an important role in the sustainable transformation of the energy system by producing environmentally friendly power. However, the variable and uncertain generation profiles of renewable energy sources entail growing challenges in terms of power imbalances. The first step to solve this problem is the deployment of flexible gas-fired generators with faster response ability. More importantly, large-scale energy storage technologies should be adopted to store the surplus renewable energy. The P2G units that convert electricity into hydrogen and synthetic natural gas (SNG) represent a promising energy storage option [1]. The combination of gas-fired generators and P2G units greatly contributes to the penetration and flexible dispatchability of renewable energy sources. In other words, integrated electrical and gas energy systems offer a complement to intermittent renewable energy sources and therefore benefit the reduction of carbon dioxide (CO_2) emissions.

Other advantages of employing such an integrated energy system lie in the economic benefits, such as the integrated planning and operation of electrical and gas networks that yield an overall optimal result [7]–[10]. Nevertheless, the deep interdependence between the two energy vectors also represents tremendous security (or reliability) challenges. A direct example of this challenge is the U.S. large-scale loss of electric and gas service that occurred in February 2011 with unusually cold weather [3]. This event stemmed from unexpected gas failures which contributed to the loss of gas-fired generators, and the loss of reliable electric service further led to gas curtailments. Because both electrical and gas systems heavily rely on the energy supply service from the other system, any uncertainties occurring in one system would directly impact the overall economic and secure operation of the integrated energy system. To control and minimize the risks caused by massive random behaviors, there is an evident need of using analytical tools able to account for uncertainties.

Energy flow analysis for integrated electrical and gas systems is considered as the cornerstone for further studies [11], [12]. Deterministic energy flow analysis is executed under given energy suppliers, energy demands and network parameters. However, the variation of the energy flow input information is so high that deterministic analysis is no longer applicable. As such, it is desirable to view the energy flow analysis as a probabilistic problem. In the background of the deep interdependence between electrical and gas networks, the necessity of jointly analyzing the probabilistic nature of both systems is mainly due to the following issues:

1) For both electrical and gas networks, the nodal security, which determines the energy delivery ability, must be carefully monitored. Therefore, the risk that the nodal voltage (or pressure) falls outside its respective permissible limit should be quantitatively analyzed.
2) The power system security is affected by the gas system in such a way that the unavailability of adequate and timely gas delivery could result in forced offline of gas-fired generators. On the other hand, the loss of reliable electric service would also lead to the outages of electric-driven compressors. Hence, the system operators should obtain a thorough knowledge of the potential risk caused by the uncertainties in the other coupled system.

More specifically, the probabilistic energy flow analysis of integrated electrical and gas energy systems, which is an extension of the well-known power system probabilistic power flow analysis [13], should be performed to assess system variables (e.g., bus voltages, nodal pressures and branch energy flows) in the presence of varying energy flow injections.

A substantial amount of work has been performed in the area of probabilistic power flow. The methods to tackle the probabilistic power flow problem can be summarized, broadly speaking, into three categories: 1) Monte Carlo simulation (MCS) [13], 2) analytical methods [14]–[18] and 3) approximate methods [19]. MCS generates random samples for variable inputs and uses the deterministic power flow for each sample. However, a considerable computational effort is required for MCS. In contrast, analytical and approximate methods are computationally efficient. Mathematical assumptions are made for analytical methods to simplify the nonlinear relationship between input and output variables. Based on linearized power flow equations, the cumulant method combined with Gram-Charlier or Cornish-Fisher expansion was studied in [14], [15]. A multi-linear model with multiple linearization points was proposed in [16]–[18] to address the extremely high uncertainties. As for the approximate methods, point estimate methods have been most useful [19].

The primary goal of this paper is to propose a probabilistic energy flow framework of integrated electrical and gas systems. First, the energy flow formulations of electrical and gas systems are presented. Then, three aspects of couplings between both systems are considered: 1) gas-fired generators, 2) electric-driven compressors and 3) energy hubs integrated with P2G. After that, the multi-linear method proposed in [16]–[18] is designed for strongly nonlinear energy flow equations especially gas flow equations. The proposal is therefore a combination of the multi-linear method and MCS. For each sample generated from MCS, the multi-linear method is used to produce a fast and accurate energy flow solution.

The remainder of this paper is organized as follows. The steady-state energy flow formulations of integrated electrical and gas systems are described in Section II. Section III elaborates on the multi-linear MCS scheme for probabilistic energy flow analysis. Section IV illustrates the performance of the proposed multi-linear MCS method and investigates the benefits of P2G. Finally, Section V draws the conclusion.

II. Modeling of Integrated Electrical and Natural-Gas Systems

A. Power Flow Formulation of Electrical Networks

For the branch l connecting buses i and j, its active and reactive power can be formulated as follows:

$$\begin{cases} P_{\mathrm{ij}} = (g_{\mathrm{ij}} + g_{\mathrm{sh},i}) V_i^2 - g_{\mathrm{ij}} V_i V_j \cos\theta_{\mathrm{ij}} - b_{\mathrm{ij}} V_i V_j \sin\theta_{\mathrm{ij}} \\ Q_{\mathrm{ij}} = -(b_{\mathrm{ij}} + b_{\mathrm{sh},i}) V_i^2 + b_{\mathrm{ij}} V_i V_j \cos\theta_{\mathrm{ij}} - g_{\mathrm{ij}} V_i V_j \sin\theta_{\mathrm{ij}} \end{cases} \quad (1)$$

The total power flowing into and out of each bus is equal:

$$P_{G,i} - P_{L,i} = \sum_{j \in i} P_{\mathrm{ij}} \tag{2}$$

$$Q_{G,i} - Q_{L,i} = \sum_{j \in i} Q_{\mathrm{ij}} \tag{3}$$

Meanwhile, with the significant penetration of wind power, it is more desirable to operate electric power systems under the automatic generation control (AGC) [20]. Under this condition, the power imbalances between generations and loads are balanced by multiple generators (i.e., distributed slack buses) and the system frequency deviation should be added into the state variables. Equations (4)–(6) represent the adjustment of the generators' active and reactive power outputs related to the frequency deviation Δf:

$$P_G = P_{G\_\mathrm{set}} + \Delta P_G \tag{4}$$

$$\Delta P_G = -K_G \Delta f \tag{5}$$

$$Q_G = Q_{G\_\mathrm{set}} + a_Q \Delta P_G + b_Q \Delta P_G^2 \tag{6}$$

Power loads are voltage and frequency dependent. As suggested in [20], steady-state active and reactive power characteristics can be modeled by including the frequency effect in ZIP load model:

$$P_L = P_{L\_\mathrm{set}}(1 + K_P \Delta f)\left(p_P + p_I\,(V/V_{\mathrm{LB}}) + p_Z\,(V/V_{\mathrm{LB}})^2\right) \tag{7}$$

$$Q_L = Q_{L\_\mathrm{set}}(1 + K_Q \Delta f)\left(q_P + q_I\,(V/V_{\mathrm{LB}}) + q_Z\,(V/V_{\mathrm{LB}})^2\right) \tag{8}$$

where $p_P(q_P)$, $p_I(q_I)$ and $p_Z(q_Z)$ are the percentage of constant power, constant current and constant impedance in the total active (reactive) load, respectively.

B. Gas Flow Formulation of Natural-Gas Networks

In this research, the steady-state model of the gas network is adopted with an acceptable accuracy [21]. Two key features of steady-state gas flow models are as follows: 1) the pipeline gas flow is nonlinearly related to the pressure drop along transmission pipelines, and 2) the nodal gas flow balance should be strictly observed. In this regard, the energy flow formulation of gas networks is quite analogous to that of electrical networks.

For the gas pipeline *w* extending from node *m* to node *n*, the gas flow is calculated as follows [12]:

$$F_w = k_w s_{\mathrm{mn}} \sqrt{s_{\mathrm{mn}}(\pi_m^2 - \pi_n^2)} \tag{9}$$

$$s_{\mathrm{mn}} = \begin{cases} +1 & \pi_m \geq \pi_n \\ -1 & \pi_m < \pi_n \end{cases} \tag{10}$$

To reduce the nonlinearity of gas flow (9), the nodal pressure is replaced by its squared formulation, which turns (9) into:

$$F_w = k_w s_{\mathrm{mn}} \sqrt{s_{\mathrm{mn}}(\Pi_m - \Pi_n)} \tag{11}$$

where $\Pi = \pi^2$.

To compensate the pressure loss for the gas transmission, compressors are installed along the gas pipelines. The amount of power consumed by the compressor *c* is determined by the gas flow through the compressor and the compression ratio [11], [22]:

$$H_{\mathrm{c}} = B_c F_{\mathrm{c}} \left(\left(\frac{\pi_m}{\pi_n}\right)^{Z_c} - 1\right) = B_c F_{\mathrm{c}} \left(\left(\frac{\Pi_m}{\Pi_n}\right)^{Z_c/2} - 1\right) \tag{12}$$

where B_c is the constant corresponding to the design of compressor *c*, and $Z_c = 0.236$ [22]. π_m/π_n represents the compression ratio, which can be obtained from the compressor's total cost minimization model under a nonconvex feasible operating domain [23].

If the compressors are driven by gas turbines, then additional gas would be extracted from gas networks:

$$\tau_c = \alpha + \beta H_c + \gamma H_c^2 \tag{13}$$

The nodal gas flow balance can be described as follows:

$$T_S F_S - T_D F_D - T_c \tau_c = A_w F_w + A_c F_c \tag{14}$$

C. Linkage Between Electrical and Gas Networks

Three aspects of linkage between electrical and gas networks are considered in this work: 1) natural-gas fired generators, 2) electric-driven compressors and 3) energy hubs integrated with P2G.

1) Gas-Fired Generators: Gas-fired generators are power suppliers in electrical networks and gas demands in gas networks simultaneously. The relationship between gas-fired generators' gas consumption F_G and active power outputs P_G are expressed as follows:

$$F_G = \alpha_g + \beta_g P_G + \gamma_g P_G^2 \tag{15}$$

Note that the generator value point effect [24] is not considered here.

2) Electric-Driven Compressors: If compressors are driven by electricity, the energy consumed by compressors is supplied from electrical networks. Hence, electric-driven compressors can be treated as power loads in electrical networks.

3) Energy Hubs Integrated With P2G: P2G technology that converts electricity into hydrogen and SNG has been considered a promising solution to avoid the curtailment of renewable energy [1]. P2G contains two main processes: 1) the electrolysis process, which splits water into hydrogen and oxygen by using electric energy, and 2) the methanization process ($CO_2 + 4H_2 \rightarrow CH_4 + 2H_2O$), which converts the hydrogen along with CO_2 into SNG. The share of hydrogen is technically and legislatively restricted [2]. In comparison, SNG can be stored in large amounts and transported in gas networks, enabling a bi-directional energy flow between electrical and gas networks. Thus, in this paper, P2G technology means converting the electricity into SNG.

The framework of an energy hub represents the conversion and possible storage of multiple energy carriers (e.g., electricity, gas, heat, etc) [25], [26]. In Fig. 1, the energy hub containing P2G, CHP and wind power is schematically illustrated. In this energy hub, the input energy sources are electricity and gas, and the output ports are electricity and heat demands. Meanwhile, several energy conversion tech-

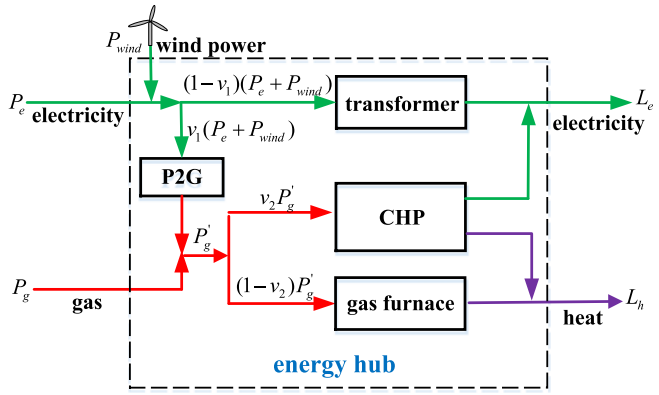

Fig. 1. The energy hub containing P2G, CHP, and wind power.

nologies are present: the transformer, P2G, CHP and the gas furnace.

The energy conversion between multiple energy inputs and outputs can be modeled as follows:

$$L_e = (P_e + P_{\text{wind}})(1 - v_1)\eta_{\text{ee}} + P_g' v_2 \eta_{\text{CHP},e} \quad (16)$$

$$L_h = P_g'(v_2 \eta_{\text{CHP},h} + (1 - v_2)\eta_{\text{gh}}) \quad (17)$$

$$P_g' = P_g + (P_e + P_{\text{wind}})v_1 \eta_{\text{eg}} \quad (18)$$

The single-period probabilistic energy flow focuses on variable energy flow injections which do not include storages. Thereby, the electrical, gas or thermal storages of energy hubs are not considered in this research. Also, the dispatch factors v_1 and v_2 represent the flexibility of energy hubs, in which demands can be supplied from alternative sources and economic benefits can be gained; but in the framework of (probabilistic) energy flow analysis, v_1 and v_2 are specified.

Note that the input electric power P_e can be either positive or negative. If the wind power is not sufficient to meet the energy demands, additional power should be supplied from the electrical network (i.e., $P_e > 0$). Otherwise, surplus wind power is injected into the electrical network (i.e., $P_e < 0$). Similarly, the input gas flow P_g, which is determined by the P2G output and the energy demands, can also be either positive or negative.

The energy hub model ((16)–(18)) can be expressed in matrix form as follows

$$\begin{bmatrix} L_e \\ L_h \end{bmatrix} = \underbrace{\begin{bmatrix} (1-v_1)\eta_{\text{ee}} + v_1\eta_{\text{eg}}v_2\eta_{\text{CHP},e} & v_2\eta_{\text{CHP},e} \\ v_1\eta_{\text{eg}}(v_2\eta_{\text{CHP},h} + (1-v_2)\eta_{\text{gh}}) & v_2\eta_{\text{CHP},h} + (1-v_2)\eta_{\text{gh}} \end{bmatrix}_C} \cdot \left(\begin{bmatrix} P_e \\ P_g \end{bmatrix} + \begin{bmatrix} P_{\text{wind}} \\ 0 \end{bmatrix} \right) \quad (19)$$

It should be clarified that we need to inverse the matrix C (assumed to square here) to calculate the input electricity/gas vector $[P_e \;\; P_g]^T$ of energy hubs. When C is a non-square matrix, virtual converters could be added into energy hubs so as to create a square matrix C [27].

D. Combined Energy Flow Formulation

Considering the coupling between electrical and gas networks, the nodal active power flow balance (2) and the nodal gas flow balance (14) are transformed into:

$$P_{G,i} - P_{L,i} - H_{c,i} - P_{e,i} = \sum_{j \in i} P_{\text{ij}} \quad (20)$$

$$T_S F_S - T_D F_D - T_c \tau_c - T_{\text{gg}} F_G - T_g P_g = A_w F_w + A_c F_c \quad (21)$$

On the basis of the energy flow formulation of the integrated electrical and gas networks ((3), (20) and (21)), the following iterative equations can be obtained using Newton's method:

$$\underbrace{\begin{pmatrix} \Delta P^{(u)} \\ \Delta Q^{(u)} \\ \Delta F^{(u)} \end{pmatrix}}_{\Delta Y} = - \underbrace{\begin{pmatrix} \frac{\partial \Delta P}{\partial \Delta f} & \frac{\partial \Delta P}{\partial \theta} & \frac{\partial \Delta P}{\partial V} & \frac{\partial \Delta P}{\partial \Pi} \\ \frac{\partial \Delta Q}{\partial \Delta f} & \frac{\partial \Delta Q}{\partial \theta} & \frac{\partial \Delta Q}{\partial V} & 0 \\ \frac{\partial \Delta F}{\partial \Delta f} & 0 & 0 & \frac{\partial \Delta F}{\partial \Pi} \end{pmatrix}^{(u)}}_{J} \underbrace{\begin{pmatrix} \Delta(\Delta f^{(u)}) \\ \Delta \theta^{(u)} \\ \Delta V^{(u)} \\ \Delta \Pi^{(u)} \end{pmatrix}}_{\Delta X} \quad (22)$$

$$X^{(u+1)} = X^{(u)} + \Delta X^{(u)} \quad (23)$$

where u is the iteration index.

After the iteration of (22)–(23) converges, the nodal pressure vector π is obtained by calculating the square root of Π.

III. Multi-Linear MCS

In this section, the linearization errors of electrical and gas energy flow equations are investigated. Then, for each sample generated by MCS, a multi-linear method is specially designed for the deterministic energy flow calculation, in which an accurate and fast result can be achieved.

A. Probabilistic Energy Flow Analysis of Integrated Electrical and Gas Networks

The probabilistic energy flow analysis proposed here is used as an analytical tool to investigate how the uncertainties of both systems can affect the overall operating states of the integrated energy systems and further provide a reference for the security and reliability evaluation of both systems.

This work takes the uncertainties of electricity, gas and heat demands and the wind power into consideration. The variations in the energy demands are modeled as correlated normal distributions, and the uncertainties of wind speeds are represented via Weibull probability distribution functions with known correlation matrix.

Meanwhile, a multi-linear MCS scheme is specially designed for the probabilistic energy flow analysis, and its detailed procedure will be illustrated in the next section.

B. Linearization Error of Power and Gas Flow Equations

1) Linearized Gas Flow: For a pipeline connecting nodes m and n, assume that the gas pipeline flow and the pressure

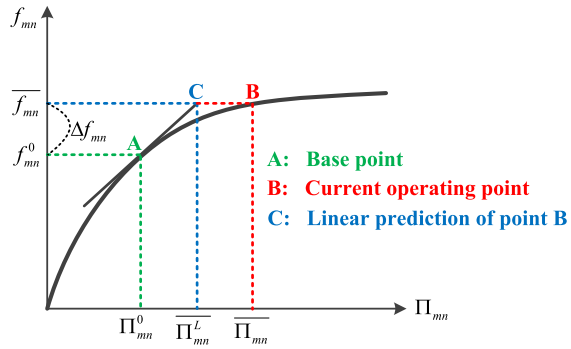

Fig. 2. The linear approximation for nonlinear gas flow equations.

of the upstream node *m* are known; the pressure of the downstream node *n* is to be determined. The diagram of linear approximation for nonlinear gas flow equations is depicted in Fig. 2.

In Fig. 2, $\Pi_{\rm mn} = \Pi_m - \Pi_n$ is the squared pressure drop (assume $\Pi_{\rm mn} > 0$). $\mathrm{A}(\Pi^0_{\rm mn}, f^0_{\rm mn})$ denotes the base point of the linear method, around which the gas flow equations are linearized. $B(\overline{\Pi_{\rm mn}}, \overline{f_{\rm mn}})$ is the current operating point, and $C(\overline{\Pi^L_{\rm mn}}, \overline{f_{\rm mn}})$ is the linear prediction of point B. The value of $\overline{\Pi_{\rm mn}}$ is calculated from the original nonlinear gas flow equations as follows:

$$\overline{\Pi_{\rm mn}} = \left(\frac{\overline{f_{\rm mn}}}{k_{\rm mn}}\right)^2 = \left(\frac{f^0_{\rm mn} + \Delta f_{\rm mn}}{k_{\rm mn}}\right)^2 = \left(\frac{f^0_{\rm mn}}{k_{\rm mn}}\right)^2 + \left(\frac{\Delta f_{\rm mn}}{k_{\rm mn}}\right)^2 + 2\frac{f^0_{\rm mn}\Delta f_{\rm mn}}{k^2_{\rm mn}} \quad (24)$$

While the value of $\overline{\Pi^L_{\rm mn}}$ is based on the linearized gas flow equations around point A as shown in (25) at the bottom of this page.

In comparing (25) with (24), the linearization error of $\overline{\Pi_{\rm mn}}$ can be obtained:

$$\overline{\Pi_{\rm mn}} - \overline{\Pi^L_{\rm mn}} = \left(\frac{\Delta f_{\rm mn}}{k_{\rm mn}}\right)^2 \quad (26)$$

On the basis of (26), the linearization error of the pressure of node *n* is given as follows:

$$\left((\overline{\pi_m})^2 - (\overline{\pi_n})^2\right) - \left((\overline{\pi_m})^2 - \left(\overline{\pi^L_n}\right)^2\right) = \left(\frac{\Delta f_{\rm mn}}{k_{\rm mn}}\right)^2$$

$$\Rightarrow \left(\overline{\pi^L_n}\right)^2 - (\overline{\pi_n})^2 = \left(\frac{\Delta f_{\rm mn}}{k_{\rm mn}}\right)^2 \quad (27)$$

$$E_{\pi_n} = \left(\overline{\pi^L_n} - \overline{\pi_n}\right)/\overline{\pi_n} = \sqrt{1 + \left(\frac{\Delta f_{\rm mn}}{k_{\rm mn}\overline{\pi_n}}\right)^2} - 1 \quad (28)$$

where $\overline{\pi_n}$ is the pressure of node *n* at the current operating point B, and $\overline{\pi^L_n}$ is the linear prediction value of $\overline{\pi_n}$. E_{π_n} is the relative linearization error of $\overline{\pi_n}$.

It can be seen from (28) that the linearization error of gas flow equations might be high in any or all of the following cases:

1) There is a major fluctuation in gas consumptions, leading to a large value of $\Delta f_{\rm mn}$.
2) Some pipelines are with long distances or high friction factor (i.e., $k_{\rm mn}$ is small).
3) The nodal pressures are low at the gas terminals during periods of peak demand (i.e., $\overline{\pi_n}$ is small).

2) Linearized Power Flow: In accordance with the branch power flow (1), the relationship between the voltage drop and the branch power flow is described as follows:

$$\mathrm{Re}\left(\dot{\Delta V}_{\rm ij}\right) = \frac{P_{\rm ij}r_{\rm ij} + Q_{\rm ij}x_{\rm ij}}{V_i} \quad (29)$$

$$\mathrm{Im}\left(\dot{\Delta V}_{\rm ij}\right) = \frac{P_{\rm ij}x_{\rm ij} - Q_{\rm ij}r_{\rm ij}}{V_i} \quad (30)$$

where $\dot{\Delta V}_{\rm ij} = V_i - V_j\angle(\theta_j - \theta_i)$

If the voltage magnitude of node *i* is constant, the voltage drop $\dot{\Delta V}_{\rm ij}$ is strictly linear with the branch power flow. However, if the value of V_i is variable, $\dot{\Delta V}_{\rm ij}$ can still be approximately seen as linear with $P_{\rm ij}$ (or $Q_{\rm ij}$) since the fluctuation range of V_i is relatively small (e.g., $0.9\ \mathrm{p.u.} \le V_i \le 1.1\ \mathrm{p.u.}$). Thereby, the approximate linear relationship between the voltage drop and branch power flow renders a relatively high accuracy of the linearized power flow equations.

3) Linearization Error Comparison: In comparing the energy flow characteristics of gas networks with that of electrical networks, two main aspects of differences can be observed:

1) There is a quadratic nonlinear correlation between the pipeline gas flow $f_{\rm mn}$ and the squared pressure drop $\Pi_{\rm mn}$ (described by (24)) while the voltage drop $\dot{\Delta V}_{\rm ij}$ is approximately linear with the branch power flow $P_{\rm ij}$ and $Q_{\rm ij}$ (described by (29) and (30)). Accordingly, the nonlinearity of $f_{\rm mn} - \Pi_{\rm mn}$ curves is much stronger than that of $P_{\rm ij}(Q_{\rm ij}) - \dot{\Delta V}_{\rm ij}$ curves.
2) Due to the wide ranges of nodal pressures (e.g., ranging from 300 Psia to 1500 Psia), the current operating point may be far away from the initial base point; but for the electrical networks, the distance between the current operating point and the initial base point is much closer.

We can conclude from the above two points that the linearization accuracy of the power flow equations is higher than that of the gas flow equations. Hence, in the combined power and gas flow analysis, special attentions should be paid to the performance of linearized gas flow models.

$$\begin{cases} \overline{\Pi^L_{\rm mn}} = \Pi^0_{\rm mn} + \Delta f_{\rm mn} / \left.\dfrac{\partial f_{\rm mn}}{\partial \Pi_{\rm mn}}\right|_0 \\ \left.\dfrac{\partial f_{\rm mn}}{\partial \Pi_{\rm mn}}\right|_0 = \dfrac{k_{\rm mn}}{2\sqrt{\Pi_{\rm mn}}} = \dfrac{k^2_{\rm mn}}{2f_{\rm mn}} \end{cases} \Rightarrow \overline{\Pi^L_{\rm mn}} = \left(\frac{f^0_{\rm mn}}{k_{\rm mn}}\right)^2 + 2\frac{f^0_{\rm mn}\Delta f_{\rm mn}}{k^2_{\rm mn}} \quad (25)$$

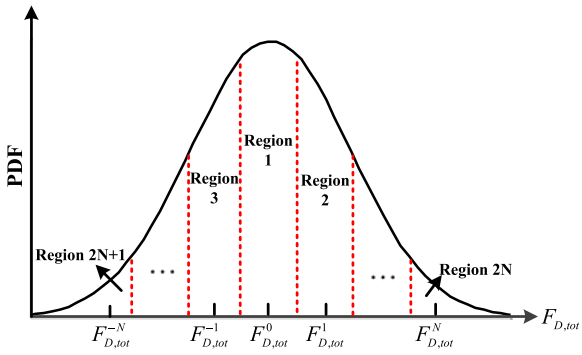

Fig. 3. The definition of different linearization regions.

C. Multi-Linear Method

For electrical networks, the linear method is applicable if the uncertainty is within a normal range [14], [15]; however, when electrical networks are faced with an extremely high level of uncertainty, the multi-linear method would be a better choice as suggested in [16]–[18]. As for gas networks, even if the uncertainty level is not high, it is still more desirable to employ the multi-linear method considering the strong nonlinearity of gas flow equations.

Multiple linearization points are designed in the multi-linear method. For a specific network injection, the linearization point closest to the current operating point would be selected. As long as the selected linearization point is close enough to the current operating point, the nonlinear energy flow equations can be locally treated as linear equations. In this way, the multi-linear method with multiple linearization points is more accurate than the linear method.

The fundamental procedure of the multi-linear method is the determination of different linearization points. As the linearization accuracy of the gas flow equations is of greater concern than power flow equations, the determination of multiple linearization points should give priority to the operating conditions of gas networks rather than electrical networks. In this way, the total equivalent gas demand is used as the criterion to determine the linearization point. In accordance with the gas flow (21), the total equivalent gas demand $F_{D,\mathrm{tot}}$ is given as:

$$F_{D,\mathrm{tot}} = \sum (T_D F_D + T_c \tau_c + T_{\mathrm{gg}} F_G + T_g P_g) \tag{31}$$

Multiple linearization points (or regions) corresponding to different gas demand levels are defined based on the probability density function (PDF) of the random variable $F_{D,\mathrm{tot}}$, as shown in Fig. 3. The determination of multiple linearization points and regions consists of the following steps:

1) For a specified number of linearization points, $F_{D,\mathrm{tot}}^{0}$ and $F_{D,\mathrm{tot}}^{N}$ can be determined according to the PDF of $F_{D,\mathrm{tot}}$ as follows:

$$\mathrm{Pro}(F \le F_{D,\mathrm{tot}}^{0}) = \frac{1}{2} \tag{32}$$

$$\mathrm{Pro}(F \le F_{D,\mathrm{tot}}^{N}) = \frac{1}{2} + \frac{N}{2(N+1)} \tag{33}$$

2) Calculate the half of the linearization region width $L_{D,\mathrm{tot}}$ as given in (34)

$$L_{D,\mathrm{tot}} = (F_{D,\mathrm{tot}}^{N} - F_{D,\mathrm{tot}}^{0})/(2N). \tag{34}$$

3) On the basis of $F_{D,\mathrm{tot}}^{0}$, $F_{D,\mathrm{tot}}^{N}$ and $L_{D,\mathrm{tot}}$, $2N+1$ linearization points $\{F_{D,\mathrm{tot}}^{-N}, \ldots, F_{D,\mathrm{tot}}^{-1}, F_{D,\mathrm{tot}}^{0}, F_{D,\mathrm{tot}}^{1}, \ldots, F_{D,\mathrm{tot}}^{N}\}$ are defined as given in (35). Further, by specifying the ratio of electricity/gas/heat demands and wind power outputs to the total equivalent gas demand, energy flow injection of all linearization points can be finally determined

$$\begin{aligned} &F_{D,\mathrm{tot}}^{-N} = F_{D,\mathrm{tot}}^{0} - 2N \cdot L_{D,\mathrm{tot}},\ F_{D,\mathrm{tot}}^{N} = F_{D,\mathrm{tot}}^{0} + 2N \cdot L_{D,\mathrm{tot}} \\ &\quad\vdots \qquad\qquad\qquad\qquad \vdots \\ &F_{D,\mathrm{tot}}^{-1} = F_{D,\mathrm{tot}}^{0} - 2L_{D,\mathrm{tot}},\ F_{D,\mathrm{tot}}^{1} = F_{D,\mathrm{tot}}^{0} + 2L_{D,\mathrm{tot}} \end{aligned} \tag{35}$$

4) Finally, the PDF of $F_{D,\mathrm{tot}}$ is divided into $2N+1$ linearization regions $\{R_1, R_2, R_3, \ldots R_{2N}, R_{2N+1}\}$ as follows:

$$\begin{aligned} R_1 &\rightarrow \{F_{D,\mathrm{tot}} | F_{D,\mathrm{tot}}^{0} - L_{D,\mathrm{tot}} \le F_{D,\mathrm{tot}} \le F_{D,\mathrm{tot}}^{0} + L_{D,\mathrm{tot}}\} \\ R_2 &\rightarrow \{F_{D,\mathrm{tot}} | F_{D,\mathrm{tot}}^{1} - L_{D,\mathrm{tot}} \le F_{D,\mathrm{tot}} \le F_{D,\mathrm{tot}}^{1} + L_{D,\mathrm{tot}}\} \\ R_3 &\rightarrow \{F_{D,\mathrm{tot}} | F_{D,\mathrm{tot}}^{-1} - L_{D,\mathrm{tot}} \le F_{D,\mathrm{tot}} \le F_{D,\mathrm{tot}}^{-1} + L_{D,\mathrm{tot}}\} \\ &\cdots\cdots \\ R_{2N} &\rightarrow \{F_{D,\mathrm{tot}} | F_{D,\mathrm{tot}} \ge F_{D,\mathrm{tot}}^{N} - L_{D,\mathrm{tot}}\} \\ R_{2N+1} &\rightarrow \{F_{D,\mathrm{tot}} | F_{D,\mathrm{tot}} \le F_{D,\mathrm{tot}}^{-N} + L_{D,\mathrm{tot}}\} \end{aligned} \tag{36}$$

Once the linearization points are determined, the nonlinear energy flow calculation for each linearization point will be performed, and the results of state variables and the inverse of the Jacobian matrices should be retained. Then, the state variables of the current operating point can be calculated around the nearest linearization point in reference to (22):

$$\overline{X^L} - X_k = -(J_k)^{-1}(\overline{Y} - Y_k) \quad \overline{F_{D,\mathrm{tot}}} \in R_k \tag{37}$$

where $\overline{F_{D,\mathrm{tot}}}$ and $\overline{Y}$ are the total equivalent gas demand and energy flow injection of the current operating point, respectively. $\overline{X^L}$ denotes the state variable vector of the current operating point obtained from the multi-linear method. X_k, Y_k and J_k represent the state variable, energy flow injection and Jacobian matrix of R_k, respectively.

As we can observe from (37), the multi-linear algorithm, without any iterative processes, is substantially more computationally efficient than the calculation of nonlinear energy flow equations by using Newton's method. Moreover, the multi-linear algorithm's accuracy is guaranteed as different gas demand levels of linearization points are designed.

It is important to clarify that the equivalent gas demands corresponding to gas-fired generators and gas-driven compressors are unknown before the solution to the energy flow equations is obtained. To minimize this problem, the amount

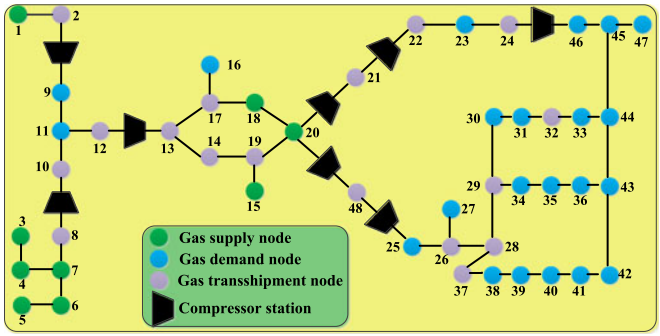

Fig. 4. Schematic of the NGS48-node system.

TABLE I
INTERDEPENDENCE BETWEEN IEEE39-NODE AND NGS48-NODE SYSTEMS

Unit	Electrical bus	Gas node
Gas-fired generator 1	31	23
Gas-fired generator 2	32	46
Gas-fired generator 3	39	25
Electric-driven compressor 1	7	(20, 21)
Electric-driven compressor 2	6	(21, 22)
Electric-driven compressor 3	7	(20, 48)
Electric-driven compressor 4	9	(48, 25)
Energy hub 1	16	34
Energy hub 2	17	35
Energy hub 3	25	26
Energy hub 4	26	43
Energy hub 5	24	30
Energy hub 6	23	31

of gas extracted by gas-fired generators (or gas-driven compressors) is assumed as a pre-specified percentage of the sum of the active power demand P_L (or the sum of the gas demand F_D). After the multi-linear algorithm is firstly performed, the value of $F_{D,\mathrm{tot}}$ is updated, followed by a second execution of the multi-linear procedure.

IV. CASE STUDIES

A. Test System Description

An integrated energy system composed of the IEEE39-node system [28] and the NGS48-node system (as shown in Fig. 4) [23] is analyzed to illustrate the performance of the proposed method. The interdependence between the electrical and gas networks is presented in Table I (the structure of energy hubs is as shown in Fig. 1). The standard deviations (SDs) of electricity/gas/heat demands are equal to 7% of their expected values (EVs). The correlation coefficients of electricity demands, gas demands, heat demands and wind speeds are set as 0.7, 0.7, 0.7 and 0.8, respectively. Detailed parameters of the test system can be found in Appendix.

It can be inferred from the test system that the installed capacities of the wind power and gas-fired generators are 16.9% and 27.8% of the total installed power generation capacities, respectively.

B. The Performance of Multi-Linear MCS

1) Linearization Error of Energy Flow Equations: The base point of the linear method corresponds to the operating condition with all random variables at their expected values. As for the multi-linear method, it contains 15 linearization points.

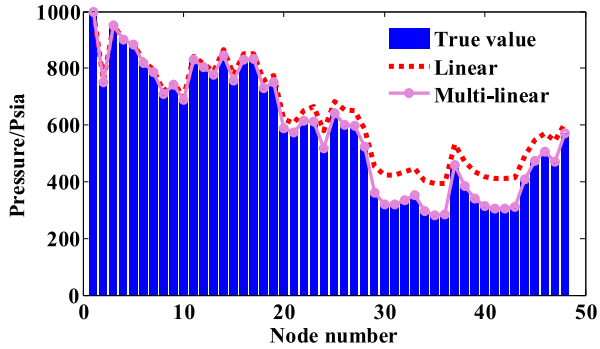

Fig. 5. The comparison of nodal pressures obtained from the linear and multi-linear schemes.

TABLE II
MCS RESULTS OF GAS NETWORKS

Error / Methods	ε_u^{π} /%		ε_σ^{π} /%	
	Mean	Max	Mean	Max
Linear MCS	0.641	1.17	1.837	4.187
Multi-linear MCS	0.008	0.017	0.240	0.356

ε_u^{π} and ε_σ^{π} represent the average relative errors of the EV and SD of nodal pressures, respectively.

TABLE III
MCS RESULTS OF ELECTRICAL NETWORKS

Error / Methods	ε_u^{V} /%		ε_σ^{V} /%	
	Mean	Max	Mean	Max
Linear MCS	0.014	0.027	0.052	0.221
Multi-linear MCS	0.024	0.045	0.074	0.331

ε_u^{V} and ε_σ^{V} denote the average relative errors of the EV and SD of nodal voltage magnitude, respectively.

An increase in the energy demands is assumed as follows: 1) electricity and heat demands are increased by 15% for all nodes, and 2) non-power-generator gas demands are increased by 7% for nodes 9, 11 and 16, 17% for nodes 23, 25 and 27, 10% for nodes 30–36 and 5% for nodes 38–47. The comparison of nodal pressures obtained from the linear and multi-linear schemes is depicted in Fig. 5. As shown in Fig. 5, the multi-linear method outweighs the linear method regarding the linearization accuracy. The low accuracy of the linear method is owing to two factors: 1) the base point is far away from the true operating point, and 2) the high gas demands render a low nodal pressure. As for the linearization error of power flow equations, the maximum and mean voltage magnitude errors of the linear method are, respectively, 0.12% and 0.06%, indicating a much lower linearization error of power flow equations in comparison with gas flow equations.

2) MCS Results: MCS is performed with a sample size of 10 000. EV, SD and the values with probabilities less than 0.05 and 0.95 are taken as the probabilistic indices. Tables II–IV summarize the probabilistic indices of the linear and multi-linear MCS schemes using the nonlinear MCS results as a reference.

TABLE IV
MCS RESULTS OF SOME ELECTRICAL AND GAS NODES

Indices	Methods	Probability <0.05	Probability <0.95
Pressure of node 35/Psia	Nonlinear MCS	541.7	1304.6
	Linear MCS	581.3	1330.2
	Multi-linear MCS	541.2	1305.5
Voltage magnitude of node 17/pu	Nonlinear MCS	1.0210	1.0382
	Linear MCS	1.0215	1.0385
	Multi-linear MCS	1.0216	1.0386
Voltage angle of node 17/rad	Nonlinear MCS	–0.1348	–0.0409
	Linear MCS	–0.1345	–0.0414
	Multi-linear MCS	–0.1346	–0.0412

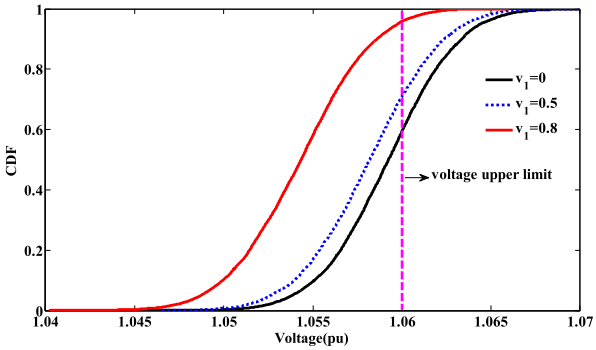

Fig. 6. The impact of P2G on the voltage magnitude of bus 25.

It can be observed from Tables II–IV that the multi-linear method provides accurate estimates for different combinations of stochastic electricity/gas/heat demands and wind power. However, the linear MCS method cannot effectively evaluate the impact of varying energy flow injections to gas networks.

3) Computational Efficiency: The simulation is performed on a 32-bit PC with 1.9-GHz CPU and 4.0-GB RAM in MATLAB environment. The computation times of MCS obtained from the nonlinear energy flow calculation, the linear method, and the multi-linear method are 486, 15 and 19 s, respectively. Since both electrical and gas transmission systems are large-scale networks, the computational cost of the integrated energy system would be challenging. Fortunately, the high computational efficiency of the multilinear MCS method could greatly alleviate this problem.

To summarize, regarding the linearization error and computational efficiency, the test results corroborate that the proposed multi-linear MCS method can produce a fast and accurate probabilistic result.

C. Positive Effects of P2G on Electrical Networks[1]

Under the variability of wind power and electricity loads, the security constraints of electricity networks cannot always be satisfied especially when high wind power outputs and low electricity loads occur simultaneously. Fig. 6 shows the variation of the cumulative distribution function (CDF) of the voltage magnitude of bus 25 with respect to the increase of v_1. When $v_1 = 0$ (i.e., P2G is not employed), the likelihood that

[1]In Section IV, the P2G units are only considered in Parts C and D.

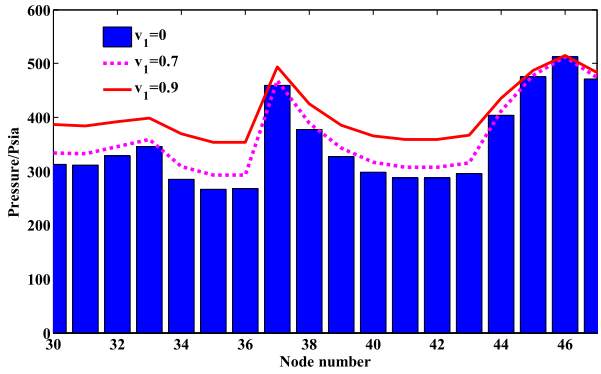

Fig. 7. The impact of P2G on the pressures of nodes 30–47.

the voltage magnitude of bus 25 exceeds its upper limit is up to 40%. Traditionally, large amounts of wind power should be curtailed to accommodate the security constraints. However, with an increased value of v_1, the otherwise curtailed wind power can be fed into P2G and further converted into natural gas. Consequently, the insecurity risk is decreased from 40% to 29% for $v_1 = 0.5$ and to 4% for $v_1 = 0.8$.

Accordingly, the P2G technology positively contributes to the reduction of wind power curtailment and the congestion relief in the electrical network.

D. Positive Effects of P2G on Gas Networks

For the gas network, P2G can be taken as an additional gas reserve. When gas sources and gas storages are struggling with the difficulties to meet the gas demands during peak periods, additional gas could be extracted from P2G. When gas demands are increased by 12%, the impact of P2G on gas node pressures of gas networks is presented in Fig. 7. As shown in Fig. 7, by injecting more gas into the gas network extremities, the pressures of nodes 30–47 are increased accordingly.

In this way, P2G is an alternative to gas network reinforcement. Meanwhile, the use of renewable natural gas (originally produced from wind power) could reduce overall CO_2 emissions from the gas sector.

As verified in Figs. 6 and 7, P2G positively contributes to the secure operation of integrated electrical and gas systems. The variation of nodal voltages or pressures under different values of v_1 could be regarded as the sensitivities of network security constraints with respect to v_1. In this sense, P2G units are potentially corrective control actions to avoid insecure operating conditions. That is to say, the network security enhancement could be achieved by adjusting the value of v_1. On the other hand, in the framework of optimal energy flow, v_1 is an important decision variable so as to obtain an economical and secure operating manner.

E. Electricity-Gas, Electricity-Heat and Gas-Heat Demand Correlations

The test results illustrated above only considers the correlation of electricity, gas or heat demand itself, but the correlation between different types of demands has not been taken into account.[2] Four cases are thereby defined with different values of electricity-gas, electricity-heat and gas-heat demand correlation coefficients as follows:

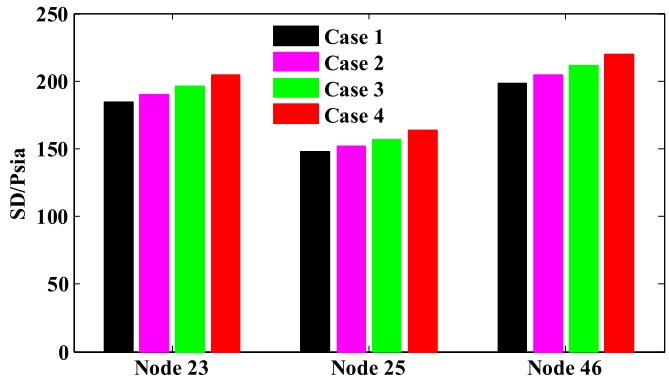

Fig. 8. SDs of some gas node pressures for Cases 1–4.

1) Case 1: $\rho_1 = \rho_2 = \rho_3 = 0$ (i.e., base case);
2) Case 2: $\rho_1 = \rho_2 = 0.3$, $\rho_3 = 0.5$;
3) Case 3: $\rho_1 = \rho_2 = 0.5$, $\rho_3 = 0.7$;
4) Case 4: $\rho_1 = \rho_2 = 0.7$, $\rho_3 = 0.8$.

Fig. 8 depicts the SDs of the pressures of gas nodes 23, 25 and 46. Fig. 8 indicates that, from Case 1 to Case 4, the fluctuation level of gas node pressures gradually increases. This is because a larger correlation coefficient results in a higher probability that peak electricity, gas and heat demands occur simultaneously.

In reality, the circumstance that peak electricity loads coincide with peak gas/heat demands poses a non-negligible threat to the integrated energy system because of the low redundancy in the gas supply infrastructure feeding gas-fired generators and the limited gas reserves provided by P2G. This potential risk underscores the necessity that the correlation between electricity, gas and heat demands should be adequately analyzed based on historical load data.

V. Conclusion

A probabilistic energy flow analysis framework for integrated electrical and gas systems has been proposed in this paper. The energy hub integrated with P2G is considered. Moreover, a multi-linear scheme is specially designed to address the concern regarding the linearization error of gas energy flow equations. Based on the test results, benefits of the proposed methodology can be summarized as:

1) The linearization error of power and gas flow equations is quantitatively investigated; it is found that the accuracy of linearized gas flow equations is of concern, whereas linearized power flow equations are applicable.
2) With multiple linearization points, the multi-linear method can rapidly yield accurate results for different combinations of energy flow injections. This leads to a precise and fast probabilistic result obtained from the proposed multi-linear MCS scheme.
3) The P2G units positively contribute to supporting the variability of wind power and providing an additional gas supply to gas terminals during peak demands. Thus, the P2G units are suggested to be located at the congested electrical buses or vulnerable gas nodes.
4) The proposed method would enable the system operators to be aware of the integrated energy system in a broader sense and further provide valuable information for the security and reliability assessment of integrated energy systems.

[2]In Section IV, only Part E considers the correlation between different types of demands.

Appendix

Parameters of gas-fired generators: $\beta_g = 0.16$MMCFD/MW, $\alpha_g = \gamma_g = 0$.

Parameters of energy hubs: $L_e = 50$ MW, $L_h = 80$ MW, $v_1 = 0$, $v_2 = 0.5$, $\eta_{\rm ee} = 0.99$, $\eta_{\rm gh} = 0.9$, $\eta_{\rm eg} = 0.6$, $\eta_{{\rm CHP},e} = 0.3$, $\eta_{{\rm CHP},h} = 0.4$.

The installed capacity of the wind farm is 250 MW. The Weibull distribution is with a scale parameter of 10.7 and a shape parameter of 3.97. The cut in, rated, and cut out speeds for the wind turbine are 3, 15 and 25 m/s, respectively.

The power generators and loads are dependent on frequency and voltage with the following parameters: $K_G^* = 25$, $K_Q = 0$, $K_L^* = 2$, $a_Q = b_Q = 1$, $P_p = Q_p = 0.2$, $P_I = Q_I = 0.3$, and $P_Z = Q_Z = 0.5$.

Network parameters of the NGS-48 node system can be found in [29].

References

[1] G. Guandalini, S. Campanari, and M. C. Romano, "Power-to-gas plants and gas turbines for improved wind energy dispatchability: Energy and economic assessment," *Appl. Energy*, vol. 147, pp. 117–130, Jun. 2015.
[2] S. Clegg and P. Mancarella, "Integrated modeling and assessment of the operational impact of power-to-gas (P2G) on electrical and gas transmission networks," *IEEE Trans. Sustain. Energy*, vol. 6, no. 4, pp. 1234–1244, Oct. 2015.
[3] P. J. Hibbard and T. Schatzki, "The interdependence of electricity and natural gas: Current factors and future prospects," *Electr. J.*, vol. 25, no. 4, pp. 6–17, May 2012.
[4] M. Qadrdan, J. Wu, N. Jenkins, and J. Ekanayake, "Operating strategies for a GB integrated gas and electricity network considering the uncertainty in wind power forecasts," *IEEE Trans. Sustain. Energy*, vol. 5, no. 1, pp. 128–138, Jan. 2014.
[5] Z. Wei, S. Chen, G. Sun, D. Wang, Y. Sun, and H. Zang, "Probabilistic available transfer capability calculation considering static security constraints and uncertainties of electricity-gas integrated energy systems," *Appl. Energy*, vol. 167, pp. 305–316, Apr. 2016.
[6] A. Quelhas, E. Gil, J. D. McCalley, and S. M. Ryan, "A multiperiod generalized network flow model of the U.S. integrated energy system: Part I—Model description," *IEEE Trans. Power Syst.*, vol. 22, no. 2, pp. 829–836, May 2007.
[7] C. Unsihuay-Vila, J. W. Marangon-Lima, A. C. Zambroni de Souza, I. J. Perez-Arriaga, and P. P. Balestrassi, "A model to long-term, multiarea, multistage, and integrated expansion planning of electricity and natural gas systems," *IEEE Trans. Power Syst.*, vol. 25, no. 2, pp. 1154–1168, May 2010.
[8] C. Correa-Posada and P. Sanchez-Martin, "Security-constrained optimal power and natural-gas flow," *IEEE Trans. Power Syst.*, vol. 29, no. 4, pp. 1780–1787, Jul. 2014.
[9] X. Xu, H. Jia, D. Wang, D. C. Yu, and H-D. Chiang, "Hierarchical energy management system for multi-source multi-product microgrids," *Renew. Energy*, vol. 78, pp. 621–630, Jun. 2015.
[10] J. Qiu, Z. Dong, J. Zhao, K. Meng, F. Luo, and Y. Chen, "Expansion co-planning for shale gas integration in a combined energy market," *J. Mod. Power Syst. Clean Energy*, vol. 3, no. 3, pp. 302–311, Mar. 2015.
[11] A. Martinez-Mares and C. R. Fuerte-Esquivel, "A unified gas and power flow analysis in natural gas and electricity coupled networks," *IEEE Trans. Power Syst.*, vol. 27, no. 4, pp. 2156–2166, Nov. 2012.
[12] A. Martinez-Mares and C. R. Fuerte-Esquivel, "Integrated energy flow analysis in natural gas and electricity coupled systems," in *Proc. IEEE North Amer. Power Symp.*, Aug. 2011, pp. 1–7.

[13] M. Aien, M. Rashidinejad, and M. Fotuhi-Firuzabad, "On possibilistic and probabilistic uncertainty assessment of power flow problem: A review and a new approach," *Renew. Sustain. Energy Rev.*, vol. 37, pp. 883–895, Sep. 2014.
[14] P. Zhang and S. T. Lee, "Probabilistic load flow computation using the method of combined cumulants and Gram-Charlier expansion," *IEEE Trans. Power Syst.*, vol. 19, no. 1, pp. 676–682, Feb. 2004.
[15] J. Usaola, "Probabilistic load flow in systems with wind generation," *IET Gener. Transm. Distrib.*, vol. 3, no. 12, pp. 1031–1041, Dec. 2009.
[16] A. M. Leite da Silva and V. L. Arienti, "Probabilistic load flow by a multilinear simulation algorithm," *Proc. Inst. Elect. Eng. C: Gener., Transm., Distrib.*, vol. 137, no. 4, pp. 276–282, Jul. 1990.
[17] G. Carpinelli, P. Caramia, and P. Varilone, "Multi-linear Monte Carlo simulation method for probabilistic load flow of distribution systems with wind and photovoltaic generation systems," *Renew. Energy*, vol. 76, pp. 283–295, Apr. 2015.
[18] G. Carpinelli, V. Di Vito, and P. Varilone, "Multi-linear Monte Carlo simulation for probabilistic three-phase load flow," *Eur. Trans. Elect. Power*, vol. 17, pp. 1–19, Feb. 2007.
[19] J. M. Morales and J. Pérez-Ruiz, "Point estimate schemes to solve the probabilistic power flow," *IEEE Trans. Power Syst.*, vol. 22, no. 4, pp. 1594–1601, Nov. 2007.
[20] L. M. Castro, C. R. Fuerte-Esquivel, and J. H. Tovar-Hernández, "Solution of power flow with automatic load-frequency control devices including wind farms," *IEEE Trans. Power Syst.*, vol. 27, no. 4, pp. 2186–2195, Nov. 2012.
[21] A. Alabdulwahab, A. Abusorrah, X. Zhang, and M. Shahidehpour, "Stochastic security-constrained scheduling of coordinated electricity and natural gas infrastructures," *IEEE Syst. J.*, to be published. [Online]. Available: http://dx.doi.org/10.1109/JSYST.2015.2423498
[22] A. Shabanpour-Haghighi and A. R. Seifi, "Effects of district heating networks on optimal energy flow of multi-carrier systems," *Renew. Sustain. Energy Rev.*, vol. 59, pp. 379–387, Jun. 2016.
[23] S. Wu, R. Z. Ríos-Mercado, E. Boyd, and L. Scott, "Model relaxation for the fuel cost minimization of steady-state gas pipeline networks," *Math. Comput. Model*, vol. 31, no. 23, pp. 197–220, Jan.-Feb. 2000.
[24] H. T. Yang, P. C. Yang, and C. L. Huang, "Evolutionary programming based economic dispatch for units with non-smooth incremental fuel cost functions," *IEEE Trans. Power Syst.*, vol. 11, no. 1, pp. 112–118, Feb. 1996.
[25] X. Zhang, M. Shahidehpour, A. Alabdulwahab, and A. Abusorrah, "Optimal expansion planning of energy hub with multiple energy infrastructures," *IEEE Trans. Smart Grid*, vol. 6, no. 5, pp. 2302–2311, Sep. 2015.
[26] F. Adamek, M. Arnold, and G. Andersson, "On decisive storage parameters for minimizing energy supply costs in multicarrier energy systems," *IEEE Trans. Sustain. Energy*, vol. 5, no. 1, pp. 102–109, Jan. 2014.
[27] M. Moeini-Aghtaie, A. Abbaspour, M. Fotuhi-Firuzabad, and E. Hajipour, "A decomposed solution to multiple-energy carriers optimal power flow," *IEEE Trans. Power Syst.*, vol. 29, no. 2, pp. 707–716, Mar. 2014.
[28] R. D. Zimmerman, C. E. Murillo-Sánchez, and R. J. Thomas, "Matpower: Steady-state operations, planning, analysis tools for power systems research and education," *IEEE Trans. Power Syst.*, vol. 26, no. 1, pp. 12–19, Feb. 2011.
[29] [Online]. Available: https://drive.google.com/open?id=0B5DUpCfGw1I5eEY0VWdVeFE2ZkU

Sheng Chen (S'15) received the Bachelor's degree from the College of Energy and Electrical Engineering, Hohai University, Nanjing, China, in 2014, where he is currently working toward the Ph.D. degree.

His research interests include economic dispatch and security analysis of integrated energy systems.

Zhinong Wei received the B.S. degree from Hefei University of Technology, Hefei, China, in 1984, the M.S. degree from Southeast University, Nanjing, China, in 1987, and the Ph.D. degree from Hohai University, Nanjing, China, in 2004.

He is currently a Professor of electrical engineering with the College of Energy and Electrical Engineering, Hohai University, Nanjing, China. His research interests include power system state estimation, integrated energy systems, smart distribution systems, optimization and planning, load forecasting, and integration of distributed generation into electric power systems.

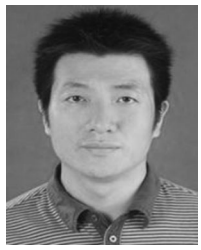

Guoqiang Sun (M'14) received the B.S., M.S., and Ph.D. degrees in electrical engineering from Hohai University, Nanjing, China, in 2001, 2005, and 2010, respectively.

He was a visiting scholar at North Carolina State University, Raleigh, NC, USA, from 2015 to 2016. He is currently an Associate Professor with the College of Energy and Electrical Engineering, Hohai University, Nanjing, China. His research interests include power system analysis and economic dispatch and optimal control of integrated energy systems.

Kwok W. Cheung (S'87–M'91–SM'98–F'14) received the Ph.D. degree in electrical engineering from Rensselaer Polytechnic Institute, Troy, NY, USA, in 1991.

He joined GE Grid Solutions (formerly ALSTOM Grid Inc.) in 1991 and is currently the Director, R&D of Network Management Solutions focusing on innovation and technology. His current interests include electricity market design and implementation, smart grid, renewable energy integration, energy forecasting, power system stability, and microgrid.

Dr. Cheung has been a registered Professional Engineer of the State of Washington since 1994.

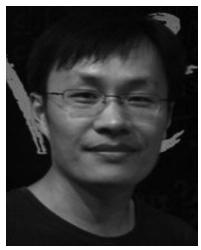

Yonghui Sun received the M.S. degree in applied mathematics from Southeast University, Nanjing, China, in 2007, and the Ph.D. degree in control theory and application from the City University of Hong Kong, Hong Kong, in 2010.

He is currently a Professor of electrical engineering with the College of Energy and Electrical Engineering, Hohai University, Nanjing, China. He is an active reviewer for many international journals. His research interests include analysis and control of power systems, stochastic control, complex networks, systems biology, and fuzzy modeling and control.